https://dx.doi.org/10.1016/j.atmosenv.2020.117429

Atmospheric nitrous acid (HONO) at a rural coastal site in North China: Seasonal variations and effects of biomass burning

Rongrong Gu[a,b], Penggang Zheng[a], Tianshu Chen[a], Can Dong[a], Ya'nan Wang[b], Yiming Liu[b], Yuhong Liu[a], Yuanyuan Luo[a], Guangxuan Han[c], Xinfeng Wang[a], Xuehua Zhou[a], Tao Wang[b], Wenxing Wang[a], Likun Xue[a,d*]

[a]Environment Research Institute, Shandong University, Qingdao, 266237, China
[b]Department of Civil and Environmental Engineering, The Hong Kong Polytechnic University, Hong Kong, 99907, China
[c]Key Laboratory of Coastal Environmental Processes and Ecological Remediation, Yantai Institute of Coastal Zone Research, Chinese Academy of Sciences, Yantai, 264003, China
[d]Ji'nan Institute of Environmental Science, Ji'nan, 250100, China

***Correspondence to*:** Likun Xue (xuelikun@sdu.edu.cn)

Abstract. Nitrous acid (HONO) plays a significant role in atmospheric chemistry due to its contribution to hydroxyl radical (OH). However, no scientific consensus has been achieved about the daytime HONO formation mechanisms. To identify the seasonal variations of HONO chemistry and the impacts of biomass burning (BB), we performed a two-phased field study in winter-spring and summer (covering a harvest season) in 2017 at a rural coastal site in North China. Though the mean HONO concentration in winter-spring (0.26±0.28 ppbv) was higher than in summer (0.17±0.19 ppbv), the maximum HONO concentrations were comparable (~2 ppbv) in the two campaigns. Both the HONO/NO_x ratio and nocturnal heterogeneous conversion efficiency of HONO (C_{HONO}) in summer were over twice of that in winter-spring. The daytime budget analysis also revealed that the strength of P_{other} (i.e., the HONO sources apart from the reaction of OH+NO) in summer was double of that in winter-spring. BB affected the HONO concentration by enhancing the contribution of heterogeneous HONO production on the aerosol surface but weakening the role of photo-related HONO formation. HONO photolysis was a significant source of OH in both winter-spring and summer, and its contribution could be further enhanced during the BB episode in summer. Our study demonstrates the significant seasonal variations of HONO and the effects of BB, and suggests needs for more multi-season observations and considerations of BB, especially during the harvest time, in HONO research.

Keywords: Nitrous acid, Seasonal variation, Biomass burning, Hydroxyl radical, North China

Graphical Abstract

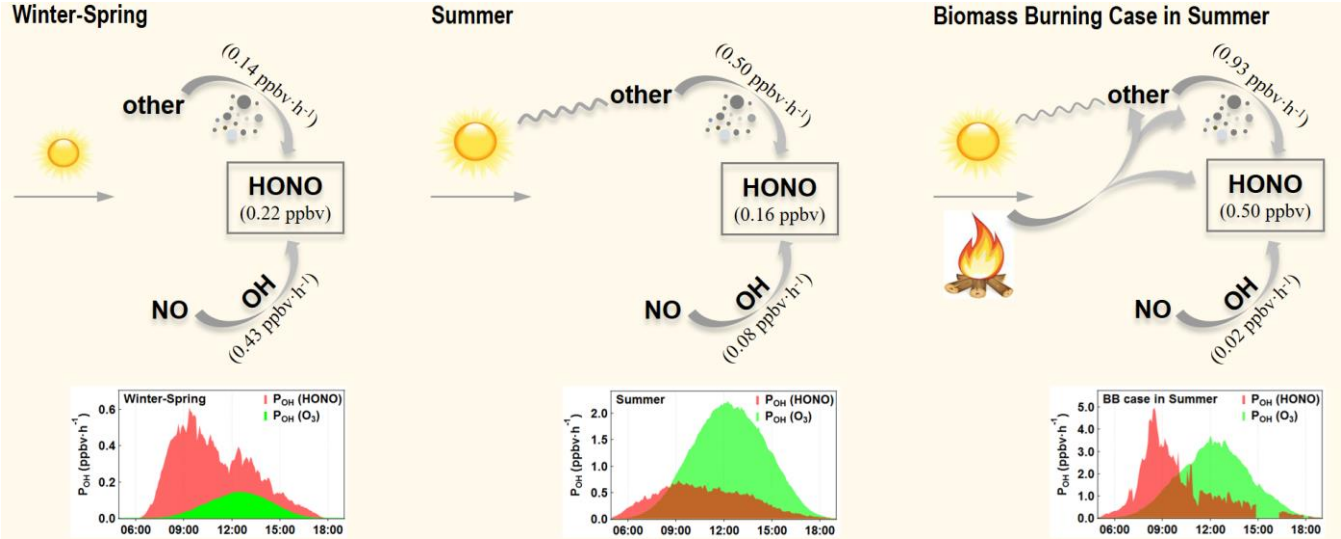

Highlights

- Significant seasonal variations of HONO pollution and chemistry were found.
- Source strength of HONO can be enhanced by solar radiation and biomass burning.
- Biomass burning enhanced the role of aerosol in heterogeneous HONO formation.

1. Introduction

Atmospheric nitrous acid (HONO) has attracted great attention in recent decades due to its contribution to the hydroxyl radical (OH) and participation in the NO_x cycle (Lammel and Cape, 1996; Ren et al., 2003; Ye et al., 2016b). OH is the major atmospheric oxidant initiating the diurnal photochemistry that can affect air quality and climate (Finlayson-Pitts and Pitts, 2000). Numerous studies have shown that the photolysis of HONO can make a significant contribution to OH not only in the early morning but also throughout the rest of the day (Acker et al., 2006b; Fu et al., 2019). Therefore, investigating the pollution characteristics and chemistry of HONO is essential for a better understanding of atmospheric chemistry and the causes of regional air pollution.

Despite the relatively good understanding of the sinks (R1, R2, and dry deposition), sources of HONO are still under debate. Tropospheric HONO sources include chemical formation and direct emissions.

$$\mathrm{HONO} + h\nu \rightarrow \mathrm{NO} + \mathrm{OH}\ (320\ \mathrm{nm} < \lambda < 400\ \mathrm{nm}) \quad \text{(R1)}$$

$$\mathrm{HONO} + \mathrm{OH} \rightarrow \mathrm{NO_2} + \mathrm{H_2O} \quad \text{(R2)}$$

The chemical reactions producing HONO include homogeneous gas-phase reactions and heterogeneous reactions on various surfaces. So far, the proposed gas-phase reaction sources of HONO include reactions R3 to R7. Among them, R4 is of minor importance due to a low HONO yield (Sörgel et al., 2011; Ye et al., 2015). R5 is still under debate due to the unconfirmed reaction rate coefficient (Carr et al., 2009; Li et al., 2008). R6 is proposed to be a non-negligible HONO source in the urban atmosphere but should be verified through more laboratory studies (Bejan et al., 2006). R7 is only proposed by density functional theory calculations, and further experimental demonstrations are needed (Zhang and Tao, 2010). The proposed heterogeneous reactions producing HONO include reactions R8 to R13. R8 is the earliest identified heterogeneous source of HONO, but it generally produces insignificant HONO because of the small reaction rate constant (Finlayson-Pitts et al., 2003). R9 is the alternative reaction of R8 and is demonstrated to be an important HONO source, but its contribution has not been accurately quantified due to the complex influences of NO_2 concentrations, moisture content, and surface characteristics on the NO_2 uptake and HONO product yield (Finlayson-Pitts et al., 2003; Sakamaki et al., 1983). R10, the heterogeneous reactions of NO_2 on the surfaces of reducing matters such as soot, humic acid, mineral

dust, and other organic substrates, can produce HONO and the production rate has been proved to be photo-enhanced (Han et al., 2017; Monge et al., 2010; Stemmler et al., 2006). In R10, 'ads' means surface-adsorbed, and 'red' and 'ox' denote the reducing matters and oxidizing substances, respectively. R11 is proposed as a HONO source in an environment surrounding with H_2O molecules but later believed to have little contribution to the ambient HONO (Kleffmann et al., 2004; Saliba et al., 2001). R12 is the photolysis and remobilization of HNO_3 and nitrate on surfaces, and it has been recognized as the dominant HONO source in the low-NO_x situation near the ground surface in daylight (Yang et al., 2018; Ye et al., 2016a; Zhou et al., 2003). Besides, the photolysis of particulate nitrate (R13) has been proposed to be a HONO source with the photolysis frequency ranging from 10^{-6} to 10^{-4} s^{-1}, which is affected by nitrate loading, organic matters, aerosol pH, and relative humidity (Ye et al., 2017; Gen et al., 2019).

$$OH + NO + M \rightarrow HONO + M \quad \text{(R3)}$$

$$HO_2 \cdot H_2O + NO_2 \rightarrow HONO + O_2 + H_2O \quad \text{(R4)}$$

$$NO_2^* + H_2O \rightarrow HONO + OH \quad \text{(R5)}$$

$$\text{ortho-nitrophenol} + h\nu \rightarrow HONO \quad \text{(R6)}$$

$$2NO_2(g) + H_2O(g) + NH_3(g) \rightarrow HONO(g) + NH_4NO_3(s) \quad \text{(R7)}$$

$$NO + NO_2 + H_2O \xrightarrow{\text{surface}} 2HONO \quad \text{(R8)}$$

$$2NO_2 + H_2O \xrightarrow{\text{surface}} HONO + HNO_3 \quad \text{(R9)}$$

$$NO_2 + \text{red}_{(ads)} \rightarrow HONO + \text{ox}_{(ads)} \quad \text{(R10)}$$

$$HNO_{3(ads)} + NO_{(g)} \rightarrow HONO + NO_2 \quad \text{(R11)}$$

$$HNO_{3(ads)}/\text{nitrate}_{(ads)} + h\nu \rightarrow HONO \quad \text{(R12)}$$

$$pNO_3 + h\nu \rightarrow HONO + NO_2 \quad \text{(R13)}$$

Direct emission sources of HONO include fossil fuel combustion (Liu et al., 2017), microbial activities in soil (Oswald et al., 2013), and biomass burning (BB) (Burling et al., 2010). While fossil fuel combustion such as vehicle exhaust is a non-negligible HONO source in urban areas (Liang et al., 2017; Yun et al., 2017), soil emissions can make a considerable contribution to ambient HONO in the areas that retain a soil cover (Oswald et al., 2013; Zhang et al., 2016). Besides, both laboratory and field studies

have shown that BB could emit HONO directly and produce HONO indirectly through heterogeneous reactions of NO_2 on soot particles (Burling et al., 2010; Yokelson et al., 2009). In a field study, direct BB emission was estimated to contribute up to 17% to the observed HONO, and heterogeneous conversion of NO_2 contributed over 80% in a nighttime BB plume (Nie et al., 2015). Despite being a significant HONO source during the harvest seasons, the BB emission of HONO has been relatively less studied so far.

In recent decades, numerous HONO field studies have been conducted around the world. Most of the observations were short-term and mono-season, and only a few long-term or multi-season measurements have been carried out. Wang et al. (2013) observed weak seasonal variations of HONO and HONO/NO_2 at an urban site in Shanghai, China. In contrast, significant monthly and seasonal differences of HONO and HONO/NO_2 were observed in some other regions. Xu et al. (2015) and Li et al. (2018) reported the maximum HONO concentrations in winter and elevated HONO/NO_2 ratio in summer at a urban site in the Pearl River Delta (PRD) and the North China Plain (NCP), respectively. In comparison, the highest HONO concentration was observed in autumn with the lowest in winter at an urban site in Beijing (Wang et al., 2017). In view of the diverse temporal variations of HONO, more multi-season field studies are needed for the comprehensive understanding of HONO pollutions, sources, and impacts on regional air quality.

To investigate the seasonal variations of HONO and the influence of BB, we carried out a two-phased field study during the winter-spring and summer (covering a harvest season) in 2017 at a rural coastal site in the Yellow River Delta (YelRD) in North China. This site is located in the warm temperate monsoon zone with four distinct seasons and limited anthropogenic activities. We present the results to show the significant seasonal variations of HONO pollution characteristics, nocturnal heterogeneous conversion coefficient (C_{HONO}), diurnal sources and sinks, and impacts on atmospheric oxidation capacity. We also analyze BB cases to highlight its important contribution to HONO during the harvest time.

2. Experiments

2.1. Study Site

The field study was carried out at the Yellow River Delta Ecology Research Station of Coastal Wetland,

Chinese Academy of Science (118.98°E, 37.76°N), which is located in the YelRD region in North China (see Figure 1). The station is surrounded by wide-open land with limited population or industrial activities within a radius of 10 km. The three closest populated areas are a town 15 km southwest, a town 20 km northwest, and a town 23 km north-northwest with resident populations of about 23,000, 46,000, and 46,000, respectively. The nearest city of Dongying is about 40 km southwest, with a population of over two million. Besides, the site is 45 km to the northeast of the Shengli Oilfield and 15 km to the southwest of the Gudong Oilfield. As the North China Plain is a major winter-wheat growing area, the air quality in this site may be affected by the wheat straw burning during the harvest season in June (Yin et al., 2019). To sum up, the station is characterized as a typical rural coastal site with distinct seasons and limited local anthropogenic emissions, but could be influenced by potential complicated transported regional air masses. More descriptions of this site were given by Zhang et al. (2019) and Zheng et al. (2019).

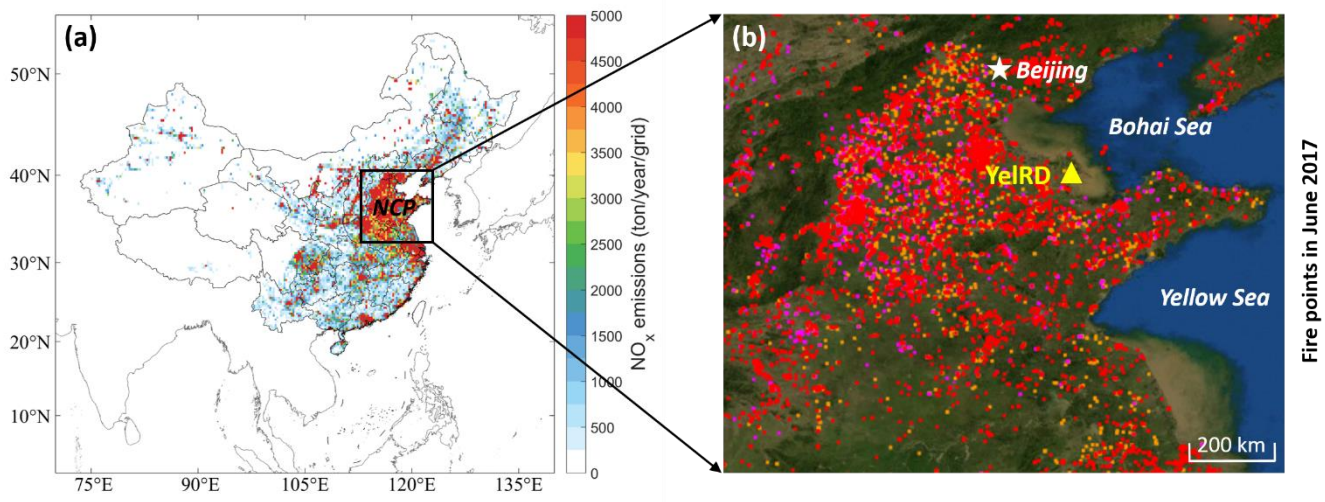

Figure 1. Maps showing (a) NCP and anthropogenic NO_x emission in China, and (b) the observation site in the YelRD and fire points in the surrounding regions. The anthropogenic NO_x emission data in 2016 in China was obtained from the MEIC (the Multi-resolution Emission Inventory for China, http://www.meicmodel.org/). The fire map of June 2017 was provided by NASA, and fire points from VIIRS, MODIS/Aqua, and MODIS/Terra were colored with red, purple, and orange, respectively (https://firms.modaps.eosdis.nasa.gov/map/). NCP and YelRD represent the regions of the North China Plain and Yellow River Delta, respectively.

2.2. Measurements

The two-phased field study was performed in the winter-spring (from February 8th to March 24th) and summer (from June 1st to July 10th) of 2017. The instruments were housed in an air-conditioned container,

and the sampling inlets were mounted on the roof-top of the container, which was about 3 m above the ground.

HONO was measured by an online commercial LOng Path Absorption Photometry instrument (LOPAP-03, QUMA, Germany) using photometric detection method (Heland et al. (2001). The collection efficiency was more than 99%, and the detection limit was 5 pptv at a time resolution of 30 s. Instrument background signals were automatically detected by sampling high purity nitrogen for 30 min every 12 h. Single-point calibrations were carried out using diluted NO_2^- standard (Nitrite Standard for IC, 1000 mg/L, Sigma-Aldrich) at a time interval of 4 days. NO and NO_y were detected with a commercial chemiluminescence analyzer (T-API Model T200U, USA), which was equipped with an externally-mounted molybdenum oxide converter. NO_2 was measured with a Cavity Attenuated Phase Shift (CAPS) detector operating as an optical absorption spectrometer (T-API Model T500U, USA). O_3 was measured by a standard UV photometric detector (TEI Model 49C, USA). CO was detected using an IR absorption analyzer equipped with a gas filter correlation wheel (T-API Model T300U, USA). $PM_{2.5}$ was measured using a synchronized hybrid ambient real-time particulate monitor (Thermo Scientific Model 5030 SHARP, USA). Meanwhile, $PM_{2.5}$ samples were collected on the quartz filter membrane (08:00-19:30 for daytime samples and 20:00-07:30 for nighttime samples) using a medium volume sampler (TH-150, Tianhong, China). Inorganic water-soluble ions (K^+, NO_3^-, NH_4^+, etc.) in the $PM_{2.5}$ samples were then analysed by an ion chromatography (ICs-90, Dionex, USA). Photolysis frequencies of HONO, NO_2, and O_3 (j(HONO), j(NO_2), and j(O^1D)) were measured with a spectro radiometer (Metcon, GmbH, Germany). Meteorological parameters (temperature, relative humidity (RH), and wind direction and speed) were monitored by a portable meteorological station (PC4, China). The time resolution of all the measurements above was 1 min except for HONO at 30 s, meteorological parameters at 5 min, $PM_{2.5}$ at 30 min, and water-soluble ions in fine particles at 11 h 30 min. More details about their detection limits, precisions, and quality assurance and quality control procedures were provided by Xue et al. (2016) and Zhang et al. (2019).

3. Results and Discussion

3.1. Seasonal and Diurnal Variations

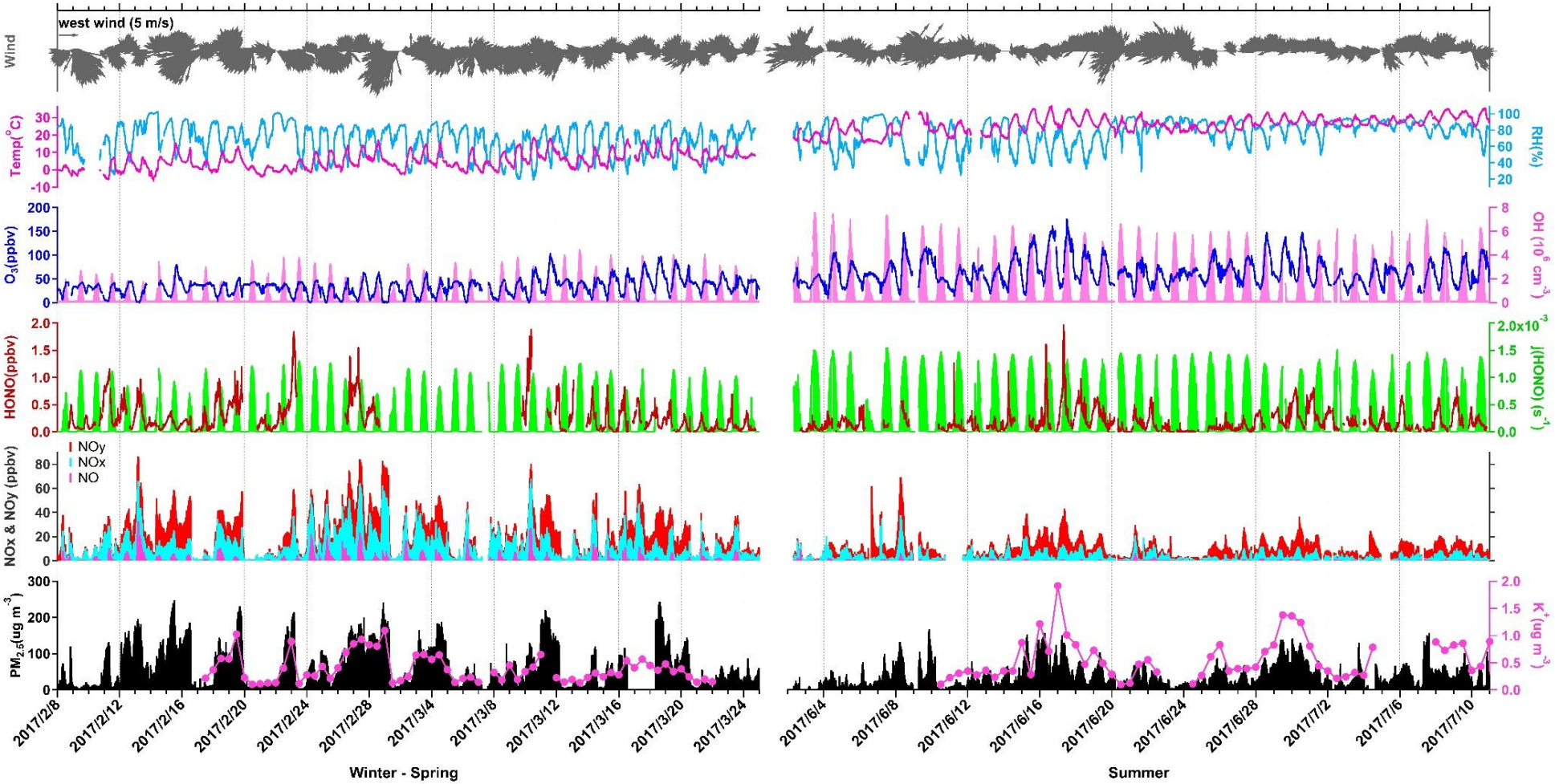

115 **Figure 2. Time series of the measured HONO, NO, NO_x, NO_y, O_3, $PM_{2.5}$, K^+ in fine particles, j(HONO), meteorological parameters, and the calculated OH during the**

116 **two-phased field study in winter-spring and summer.**

Figure 2 presents the overview of the observed HONO, related species and meteorological parameters, and the calculated OH throughout the two-phased field study. The OH concentration ([OH]) was calculated using the equation E1 with measured $j(O^1D)$ and the coefficients of $a=2.4\times10^6$ cm^{-3}, b=1, $c=0.13\times10^6$ cm^{-3}, which were proposed by Rohrer and Berresheim (2006) for rural areas. The calculated OH concentrations match well with the simulated results by the MCM model (Zhang et al., 2019). The descriptive statistics of NO, NO_2, NO_y, HONO, temperature, and RH are listed in Table 1.

$$[OH] = a \times (j(O^1D)/10^{-5}\ s^{-1})^b + c \quad \text{(E1)}$$

Table 1. Statistics of the measured HONO, NO, NO_2, NO_y, and meteorological parameters during winter-spring and summer.

	Winter-Spring						Summer					
	Min.	Max.	Med.	Mean ± SD			Min.	Max.	Med.	Mean ± SD		
				All Day	Daytime	Nighttime				All Day	Daytime	Nighttime
HONO (ppbv)	BDL	2.07	0.18	0.26±0.28	0.22±0.24	0.30±0.28	BDL	2.00	0.11	0.17±0.20	0.16±0.20	0.20±0.18
NO (ppbv)	BDL	46.92	0.17	1.49±3.28	2.91±3.71	0.33±1.95	BDL	19.03	0.17	0.32±0.50	0.43±0.61	0.16±0.20
NO_2 (ppbv)	0.32	55.34	7.86	10.41±9.11	9.85±8.10	10.50±9.70	BDL	37.32	2.37	3.47±3.34	3.41±3.68	3.48±2.64
NO_y (ppbv)	BDL	86.74	17.47	20.36±17.07	22.55±17.90	18.47±16.35	BDL	69.58	8.45	10.14±7.73	11.22±8.74	8.45±5.42
Temp. (°C)	-6.4	18.6	4.9	5.3±4.9	8.3±4.8	3.0±3.7	14.9	36.8	26.1	25.9±4.5	27.3±4.5	23.9±3.8
RH (%)	19	102	72	68±18	55±18	79±11	25	99	82	76±16	71±17	85±10

Note: The statistical analysis was based on data with time resolution of 1 min for trace species and 5 min for meteorological parameters. According to the time of sunset and sunrise throughout the experiment, the daytime was defined as 08:00-17:00 (05:00-19:00) local time for winter-spring (summer), and the nighttime was defined as 19:00-06:00 (20:00-04:00) local time for winter-spring (summer). BDL means below detection limit.

Generally, concentrations of air pollutants (except for O_3 and K^+ in fine particles) were higher in winter-spring than in summer. The average HONO concentrations were 0.26±0.28 ppbv in winter-spring and 0.17±0.20 ppbv in summer, with the maximum values of 2.07 and 2.00 ppbv, respectively. The mean HONO concentration at this rural coastal site was lower than that in other polluted rural sites in the Yangtze River Delta (YRD) (Nie et al., 2015), PRD (Li et al., 2012), and Beijing-Tianjin-Hebei region (Yang et al., 2014) in China. However, it was much higher than that in most European sites (Acker et al., 2006a; Alicke et al., 2002; Meusel et al., 2016). NO_x and NO_y, which are significant precursors of HONO, showed the mixing ratios ranging from several to tens of ppbv with much higher concentrations in winter-spring than in summer. $PM_{2.5}$ also showed a similar seasonal variation pattern with NO_x and NO_y. As a

tracer of biomass burning, K^+ in fine particles showed elevated concentrations in two episodes during June 16-17 and June 29-30 in summer with the daily average mixing ratio of more than 1 $\mu g \cdot m^{-3}$. As a secondary photochemical product, O_3 exhibited typical high levels in summer with several peaks over 150 ppbv as a result of enhanced photochemistry.

Figure 3 shows the average diurnal patterns of HONO and related species and parameters during the two-phased field study. Most of the pollutants and parameters presented similar diurnal variations in the two campaigns except for HONO/NO_x. HONO concentrations displayed a typical diurnal pattern in both campaigns, rising during the nighttime with a peak before sunrise and decreasing during the daytime with a valley around the late afternoon. The accumulation of HONO during nighttime indicated steady HONO sources at night. Given that the lifetime of HONO during midday was less than 30 min, the considerable HONO concentrations during daytime suggested the existence of significant HONO sources. Besides, despite the greater HONO photolysis and several times lower concentrations of related pollutants (NO_x, NO_y, and $PM_{2.5}$) in summer than in winter-spring, the HONO concentrations in summer were just a little lower than those in winter-spring, indicating enhanced HONO sources in summer. The NO concentrations began to rise in the late night and peaked in the early morning during both campaigns, with a much sharper and wider peak in winter-spring than in summer. The diurnal patterns of NO_2, NO_y, and $PM_{2.5}$ were similar, peaking in the morning and then decreasing to the valley in the afternoon. O_3 showed a typical diurnal pattern in both campaigns, increasing since sunrise and reaching the maximum at around 15:00 LT, and then decreasing until the next day before sunrise and reaching the minimum. The ratio of HONO/NO_x (or HONO/NO_2) has been used to characterize the heterogeneous formation of HONO from NO_2 (e.g., Xu et al., 2015). As the HONO/NO_2 ratio may be subject to interferences from direct HONO emissions, the HONO/NO_x ratio should be a more reliable parameter to indicate the efficiency of the heterogeneous NO_2-to-HONO conversion. The diurnal pattern of HONO/NO_x displayed noticeable seasonal variations. In winter-spring, it decreased since late night and reached the minimum in the late afternoon, then increased rapidly before midnight and stayed stable for a few hours until the late night. In summer, an extra peak of HONO/NO_x showed up in the midday, which was comparable to the nighttime peak. This peculiar HONO/NO_x peak indicated some enhanced HONO sources at noon in summer. A detailed discussion about the potential HONO sources in the daytime will be given in section 3.3.

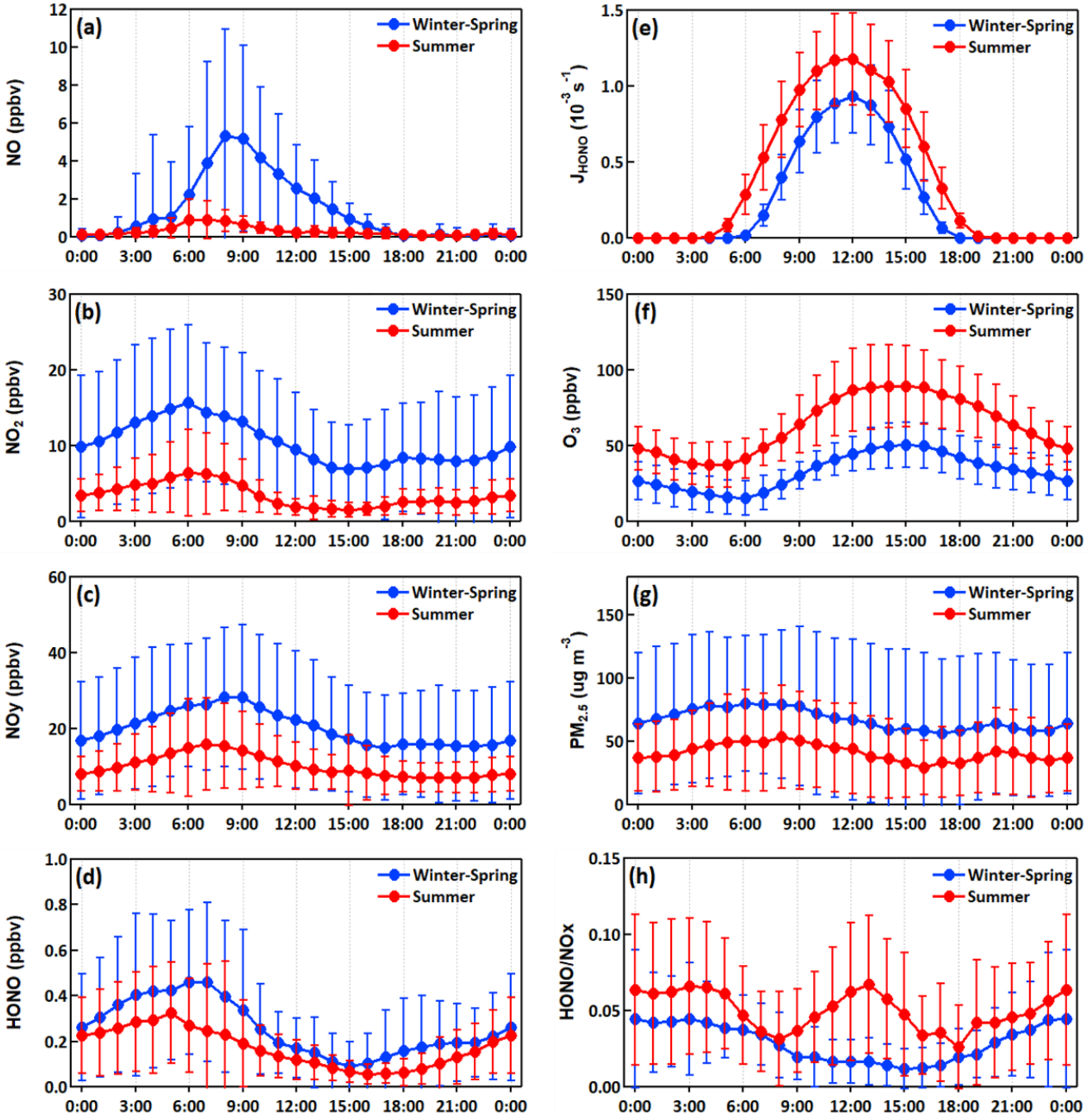

166 **Figure 3. Diurnal variations of (a) NO, (b) NO_2, (c) NO_y, (d) HONO, (e) j(HONO), (f) O_3, (g) $PM_{2.5}$, and (h) $HONO/NO_x$ during the two-phased field experiment in winter-spring and summer.** The error bars represent one
167 standard deviation.

169 ### 3.2. Nocturnal HONO Formation

170 Heterogeneous conversion of NO_2 to HONO is the commonly accepted HONO source. The HONO
171 conversion rate divided by NO_2 (C_{HONO}, h^{-1}) is a widely used scaling approach for the calculation of
172 nocturnal NO_2-to-HONO conversion frequency (Su et al., 2008a; Yu et al., 2009). Equation E2, which is
173 suitable for the C_{HONO} calculation at rural sites with little or negligible effects of vehicle emissions, is

used in this study (Su et al., 2008a). In E2, P_{HONO} is the HONO production rate with the unit of ppbv·h^{-1}, $\overline{[NO_2]}$ is the mean NO_2 concentration during time t_1 to t_2, $[HONO]_{t_{1/2}}$ is the HONO concentration at time t_1 or t_2. To calculate the C_{HONO}, several criteria were adopted for the case selection. First, only the nocturnal data were considered to avoid the complicated daytime sources and sinks of HONO. Note that the heterogeneous conversion of NO_2 to HONO is the most commonly accepted HONO source at nighttime, when both anthropogenic emissions (in particular at such a rural site in this study) and the atmospheric photochemistry are in their minimum intensity. Second, both HONO concentration and HONO/NO_2 ratio presented increasing trends for a relatively long period (e.g., more than two hours). Third, the concentrations of other pollutants (such as NO, NO_2, and CO, etc.) were stable to ensure that the air mass was consistent. Last, the weather conditions were stable with steady wind direction and small wind speeds (e.g., <3 m·s^{-1}). According to the above criteria, 10 and 7 cases were chosen for the winter-spring and summer phases, respectively, as listed in Table S1.

$$C_{HONO} = \frac{P_{HONO}}{\overline{[NO_2]}} = \frac{[HONO]_{t_2} - [HONO]_{t_1}}{(t_2 - t_1)\overline{[NO_2]}} \quad \text{(E2)}$$

The calculated C_{HONO} showed a significant variation between winter-spring and summer. While C_{HONO} ranged from 0.48 to 1.54 % h^{-1} with an average of 0.96±0.33 % h^{-1} in winter-spring, it varied from 0.90 to 4.06 % h^{-1} with a mean of 2.47±0.98 % h^{-1} in summer. C_{HONO} presented a strong correlation with ambient temperature (r=0.76) and a moderate relationship with RH (r=0.57), which was consistent with the study of Wen et al. (2019) in a marine boundary layer. The average C_{HONO} at our site was within the range of 0.43-3.36 % h^{-1} that determined from other studies around the world (Liu et al., 2019; Xu et al., 2015). Seasonal variation of C_{HONO} has also been found by Liu et al. (2019) at a suburban site in Nanjing in the subtropical zone with four distinct seasons.

3.3. Daytime HONO Formation

To investigate the strength of the daytime HONO sources and their seasonal variations, we performed a budget analysis based on the description by equation E3 (Liu et al., 2019; Su et al., 2008b). The HONO sources include direct emission from anthropogenic combustions (P_{emis}), the well-accepted homogeneous formation from reaction R3 (P_{OH+NO}), and the remaining other sources (P_{other}). The sinks of gaseous

HONO contain the homogeneous reaction of R2 ($L_{OH+HONO}$), photolysis (L_{phot}), and dry deposition (L_{dep}). In addition, vertical and horizontal transport (F_v and F_h) could affect the HONO budget as well. Assuming that no HONO was emitted from anthropogenic activity at this coastal site (considering little anthropogenic emission sources nearby) and the influence of transport was negligible (given the short lifetime of HONO during the daytime), equation E4 could be derived from E3 for the calculation of P_{other}. In E4, $k_{OH+HONO}$ denotes the reaction rate constant of reaction R2 with a value of $2.5\times10^{-12}\times\exp(260/T)$ $cm^3\cdot molecules^{-1}\cdot s^{-1}$ (Atkinson et al., 2004); k_{OH+NO} denotes the reaction rate constant of reaction R3 with a value of $7.4\times10^{-31}\times(T/300)^{-2.4}\times[N_2]$ $cm^3\cdot molecules^{-1}\cdot s^{-1}$ (Atkinson et al., 2004); ν_{HONO} is the dry deposition velocity of HONO in the daytime using an empirical value of 2 $cm\cdot s^{-1}$ (Harrison et al., 1996); H is the mixing height of HONO with an assumed value of 200 m (Alicke et al., 2002).

$$\frac{\Delta[HONO]}{\Delta t} = (P_{emis} + P_{OH+NO} + P_{other}) - \left(L_{OH+HONO} + L_{phot} + L_{dep}\right) + F_v + F_h \quad \text{(E3)}$$

$$P_{other} = j(HONO)[HONO] + k_{OH+HONO}[OH][HONO] + \frac{\Delta[HONO]}{\Delta t} + \frac{\nu_{HONO}}{H}[HONO] - k_{OH+NO}[OH][NO] \quad \text{(E4)}$$

Figure 4 shows the hourly average HONO budgets during the daytime in the winter-spring and summer campaigns. Seasonal consistencies of HONO sinks but significant seasonal differences of HONO sources were found. During both campaigns, HONO photolysis (L_{phot}) was the major loss pathway, followed by dry deposition (L_{dep}) and the negligible homogeneous reaction of R2 ($L_{OH+HONO}$). During noontime (11:00-14:00 LT) in winter-spring, the average loss rate of L_{phot}, L_{dep}, and $L_{OH+HONO}$ was 0.57, 0.07, and 0.01 $ppbv\cdot h^{-1}$, respectively. During noontime in summer, in comparison, the average loss rate of L_{phot}, L_{dep}, and $L_{OH+HONO}$ was 0.53, 0.04, and 0.01 $ppbv\cdot h^{-1}$, respectively. Despite the similar HONO sinks, the HONO sources presented significant differences between the two campaigns. In winter-spring, the homogeneous reaction of R3 (P_{OH+NO}) was the dominant HONO source with a mean production rate of 0.43 $ppbv\cdot h^{-1}$ during noontime, while P_{other} was 0.14 $ppbv\cdot h^{-1}$, accounting for 25% of the HONO production. During noontime in summer, however, the average production rate of P_{OH+NO} was only 0.08 $ppbv\cdot h^{-1}$, whilst P_{other} was up to 0.50 $ppbv\cdot h^{-1}$ and accounted for 87% of the HONO production. The strength of P_{other} during noontime at our site was at the lowest level compared with other studies, whose results ranged from 0.22 to 3.05 $ppbv\cdot h^{-1}$ (see Liu et al. (2019) and references therein). The seasonal variation of P_{other} in this study was consistent with that at an urban site in Beijing, where the value in

summer (3.05 ppbv·h^{-1}) was higher than that in spring (2.63 ppbv·h^{-1}) and winter (1.30 ppbv·h^{-1}) (Wang et al., 2017). In comparison, it differed from that at a suburban site in Nanjing where higher values occurred in spring (1.73 ppbv·h^{-1}) and winter (1.15 ppbv·h^{-1}) than in summer (1.00 ppbv·h^{-1}) (Liu et al., 2019). The varying seasonal differences of the HONO budget demonstrate that multi-season observations are required at diverse sites.

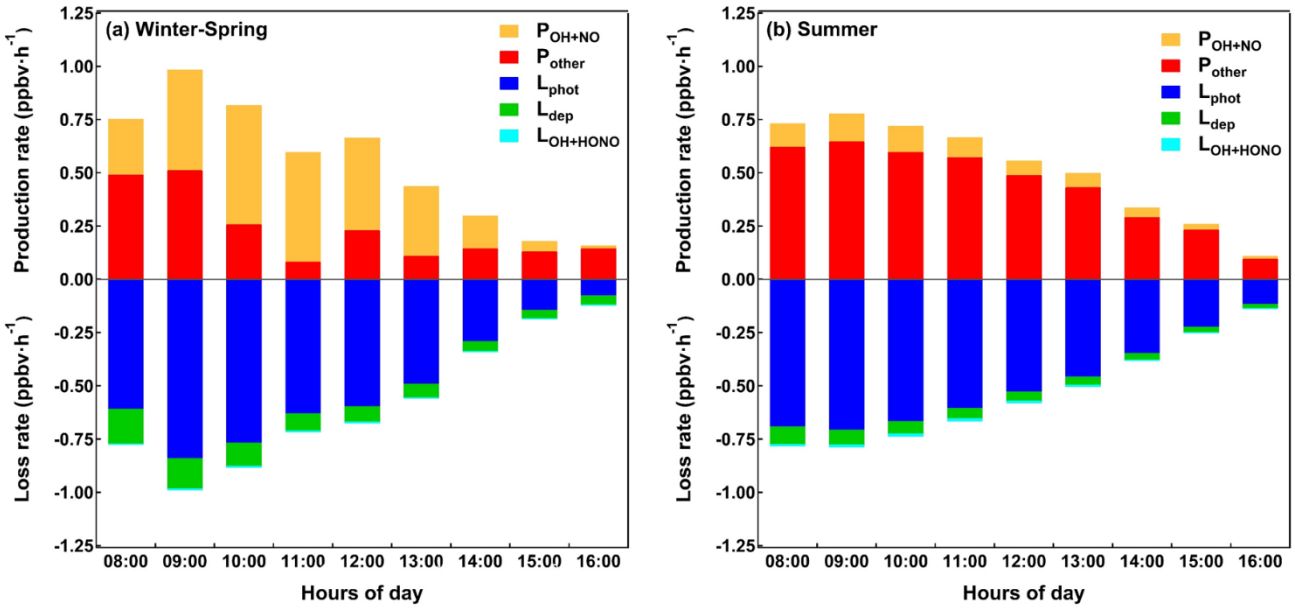

Figure 4. Hourly average HONO production and loss rates during the daytime in (a) winter-spring and (b) summer.

The elevated strength and proportion of P_{other} in summer suggest the existence of some strongly enhanced HONO source(s) in the summer season. To investigate the potential daytime HONO sources, we summarized the correlations between the daytime (08:00-17:00 LT) P_{other} with relevant trace species and meteorological parameters (see Table 2). The correlation analysis revealed different seasonal characteristics of the potential daytime HONO sources. In winter-spring, P_{other} showed no linear correlations with j(NO_2)-related parameters ($r \leq 0.1$), suggesting that the unknown HONO source in winter-spring had no relationship with the photo-related HONO formation mechanisms. And the weak positive correlations ($r < 0.3$) between P_{other} with other pollutants give no significant indications of any potential HONO source. In summer, direct emission sources were ruled out first because P_{other} showed no correlation with NO ($r = 0.09$), which is the tracer of fresh plume emitted by fuel combustion. Some studies have proposed that photo-enhanced heterogeneous reactions of NO_2 and photolysis of nitrate and nitric acid may be important daytime HONO sources (Finlayson-Pitts et al., 2003; Zhou et al., 2003; Ye et al.,

2016a). Here we examined the correlations of P_{other} with NO_2 and NOz, taking NOz as a proxy of nitrate and nitric acid (highly time resolved measurements of nitrate and nitric acid were unavailable in this study). P_{other} showed overall moderate correlations with NO_2 (r=0.47) and NO_z (r=0.57). When taking solar radiation ($j(NO_2)$ as a proxy) into consideration, the correlations became stronger, with $j(NO_2)*NO_2$ (r=0.56) and $j(NO_2)*NO_z$ (r=0.61). On one hand, the increased correlation indicates the photo-induced heterogeneous formation mechanism of HONO. On another hand, according to the correlation strength, it can be argued that the photolysis of nitrate and nitric acid as well as photo-enhanced heterogeneous conversion of NO_2 should be important HONO sources in the YelRD region. These results agree with a recent study that demonstrated aqueous phase photolysis of particulate nitrate as an important source of HONO (Gen et al., 2019).

Table 2. Correlations of the diurnal P_{other} against related pollutants and parameters.

Parameter	Total		Winter-Spring		Summer		BB case		NBB case	
	r	N	r	N	r	N	r	N	r	N
RH	-0.04	989	0.06	455	-0.24	534	0.88	29	0.08	19
$j(NO_2)$	0.24	1002	-0.10	455	0.29	547	-0.11	29	0.89	19
CO	0.23	1001	0.25	454	0.39	547	0.08	29	0.73	19
SO_2	0.22	1000	0.28	453	0.59	547	0.47	29	0.35	19
NO	0.01	1002	0.19	455	0.09	547	0.74	29	0.63	19
NO_2	0.05	1002	0.18	455	0.47	547	0.81	29	0.51	19
NO_z	0.17	1002	-0.02	455	0.57	547	0.51	29	0.36	19
$PM_{2.5}$	0.15	968	0.20	439	0.36	529	0.74	29	0.20	19
$PM_{2.5}*NO_2$	0.08	968	0.22	439	0.53	529	0.83	29	0.52	19
$PM_{2.5}*NO_z$	0.11	968	0.10	439	0.54	529	0.64	29	0.30	19
$j(NO_2)*NO_2$	0.09	1002	0.02	455	0.56	547	0.80	29	0.78	19
$j(NO_2)*NO_z$	0.30	1002	-0.14	455	0.61	547	0.38	29	0.67	19
$j(NO_2)*PM_{2.5}$	0.24	968	0.07	439	0.40	529	0.54	29	0.65	19
$j(NO_2)*NO_2*PM_{2.5}$	0.08	968	0.08	439	0.57	529	0.82	29	0.75	19
$j(NO_2)*NO_z*PM_{2.5}$	0.18	968	0.00	439	0.56	529	0.58	29	0.51	19

Note: The daytime period was set as 08:00-17:00 here following the section 3.3. The time resolution of all the data used for the correlation calculation is 30 min.

3.4. Effects of Biomass Burning

As June is the harvest month of winter wheat in North China, deteriorated air quality could happen during this period due to the wheat straw burning. As shown in Figure 2, highly elevated concentrations of HONO, K^+ in fine particles, $PM_{2.5}$, and NO_y were observed on June 16th and 17th during which the daily fire maps (see Figure S1 (https://firms.modaps.eosdis.nasa.gov)) displayed intensive fire points around North China. On June 5th, by contrast, almost no fire point was detected around our study site. Therefore, June 16th-17th was considered as the typical biomass burning (BB) case, and June 5th was considered as the none-biomass burning (NBB) case.

Significant differences in the pollution characteristics were found between the BB case and the NBB case. Figure 5 presents the diurnal variations of HONO and several relevant pollutants and parameters during the two cases. The average HONO concentration was about three times higher in the BB case (0.41±0.42 ppbv) than in the NBB case (0.14±0.07 ppbv). In the NBB case, the maximum HONO concentration occurred in the late night and was about 0.45 ppbv. In the BB case, the HONO concentration increased unusually in the early morning, and the peak went across the whole morning with a substantially elevated maximum of 1.60 ppbv on June 16th and 2.00 ppbv on 17th, which was also the maximum value observed throughout the summer campaign. While the average concentrations of NO_x were the same in both cases (both of 5.4±3.1 ppbv), the average concentration of NO_y was over two times higher in the BB case (18.6±8.2 ppbv) than in the NBB case (8.0±3.3 ppbv), indicating that the BB plume was much chemically aged than the NBB plume. The average concentration of $PM_{2.5}$ in the BB case (84.9±37.3 $\mu g \cdot m^{-3}$) was about six times higher than that in the NBB case (14.2±7.3 $\mu g \cdot m^{-3}$), implying much heavier particulate pollution, and as detailed below, aerosol played a more important role in the heterogeneous formation of HONO during the BB case. The O_3 concentration doubled in the BB case (96±42 ppbv), indicating more serious photochemistry pollution.

The strength of the other HONO sources (P_{other}), as shown in Figure S2, increased substantially in the BB case. To explore the potential HONO source and the influence of BB on HONO chemistry during this episode, Table 2 lists the correlations of P_{other} against various pollutants and parameters in the BB and NBB cases. In both cases, differing from the whole summer campaign, P_{other} presented moderate correlations with NO, indicating a considerable contribution of direct HONO emissions. In the NBB case,

P_{other} was highly correlated with j(NO_2), and all the correlations with NO_2, NO_z, and $PM_{2.5}$ increased significantly after considering the solar radiation effect. In the BB case, however, no correlation of P_{other} with j(NO_2) was found, and all the relationships with NO_2, NO_z, and $PM_{2.5}$ weakened more or less when considering the solar radiation. This phenomenon implies that the role of the photo-related heterogeneous formation mechanism of HONO was suppressed during the BB period, which should be ascribed to the dimming effect of high aerosol loading from BB emissions. Compared with the NBB case, the correlation of P_{other} with $PM_{2.5}$ drastically enhanced in the BB case, implying significantly increased effects of particles. As the indicator of particle loading, $PM_{2.5}$ could contribute to HONO chemistry through either producing HONO via the photolysis of particulate nitrate or providing the aerosol surface for HONO heterogeneous formation. Because of the weaker relationship of P_{other} with j(NO_2)*$PM_{2.5}$ compared with $PM_{2.5}$, and the stronger correlation of P_{other} with $PM_{2.5}$*NO_2 (or $PM_{2.5}$*NO_z) compared with NO_2 (or NO_z), we argue that particles may play a major role in HONO formation by providing heterogeneous reaction surface during the BB episode. It should be noted that such correlation analysis may be inherently subject to some uncertainties, and more detailed process studies are needed to better understand the HONO formation mechanisms in the BB plumes.

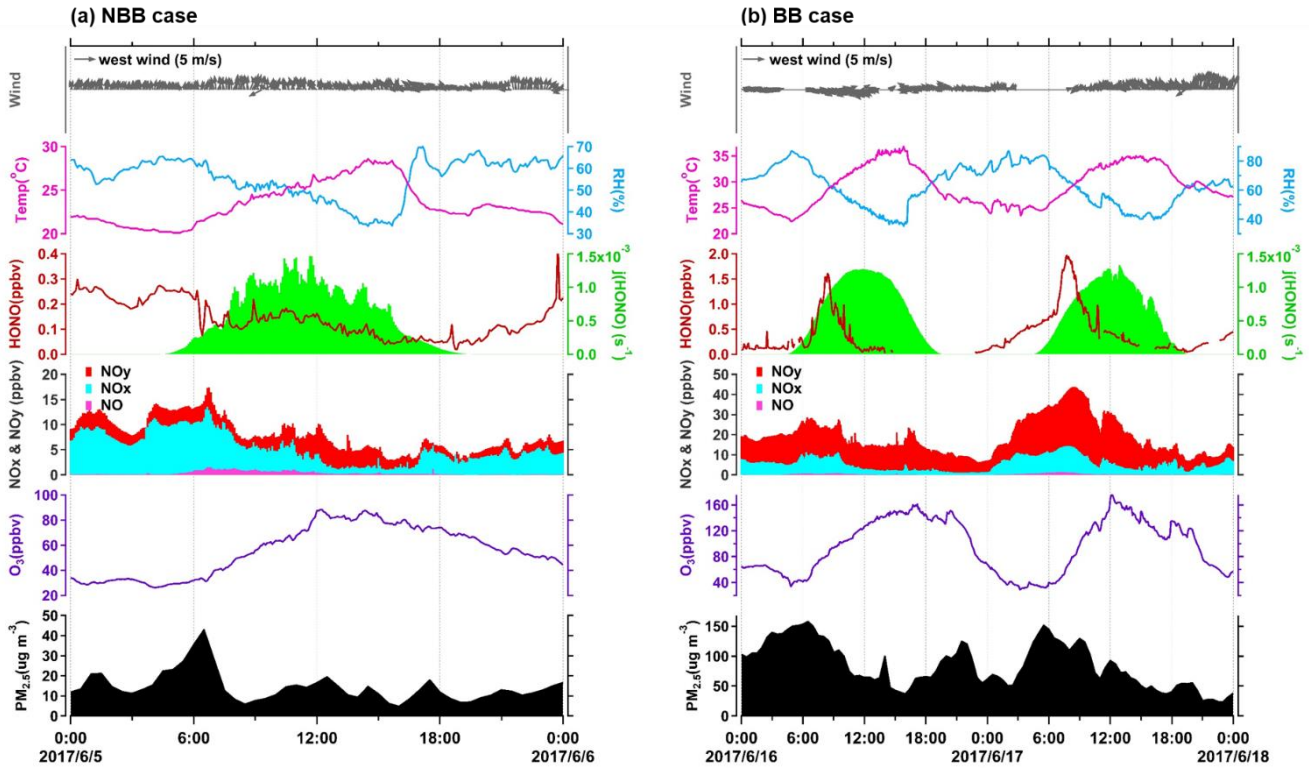

Figure 5. Diurnal variations of HONO, NO, NO_x, NO_y, O_3, $PM_{2.5}$, j(HONO), and meteorological parameters during (a) the none biomass burning (NBB) case on June 5th and (b) the biomass burning (BB) case from June 16th to 17th 2017.

3.5. Contribution to the OH Source

Photolysis of HONO can make a considerable contribution to the OH radical during the daytime. To evaluate the net OH production rate from HONO photolysis, equation E5 was used for the calculation considering the homogeneous reactions of R1 to R3. For comparison, the OH production rate from the photolysis of O_3, another significant precursor of OH, was calculated using the equation E6 based on the reactions of R14 to R16. P_{OH}(HONO) is the net OH production rate from HONO photolysis, and $P_{OH}(O_3)$ is the OH production rate from O_3 photolysis. The reaction rate constants were taken from Atkinson et al. (2004).

$$O_3 + h\nu \rightarrow O(^1D) + O_2 \ (\lambda < 340\ nm) \quad \text{(R14)}$$

$$O(^1D) + H_2O \rightarrow 2OH \quad \text{(R15)}$$

$$O(^1D) + M \rightarrow O(^3P) + M \ (M = N_2 \text{ or } O_2) \quad \text{(R16)}$$

$$P_{OH}(HONO) = j(HONO)[HONO] - k_{OH+HONO}[HONO][OH] - k_{OH+NO}[NO][OH] \quad \text{(E5)}$$

$$P_{OH}(O_3) = j(O^1D)[O_3] \cdot \frac{2k_{O(^1D)+H_2O}[H_2O]}{k_{O(^1D)+H_2O}[H_2O] + k_{O(^1D)+N_2}[N_2] + k_{O(^1D)+O_2}[O_2]} \quad \text{(E6)}$$

Figure 6(a) and (b) present the average diurnal OH production rates from photolysis of HONO and O_3 in winter-spring and summer, respectively. In winter-spring, HONO photolysis made a much greater contribution to OH than O_3 throughout the daytime, with the peak P_{OH}(HONO) of 0.61 ppbv·h^{-1} in the late morning and the peak $P_{OH}(O_3)$ of 0.15 ppbv·h^{-1} around the noon. In summer, while HONO contributed more OH than O_3 before the late morning with the peak P_{OH}(HONO) of 0.73 ppbv·h^{-1}, O_3 photolysis became the more significant OH source during the rest of the daytime with the peak $P_{OH}(O_3)$ of 2.22 ppbv·h^{-1} around the noon. On average, during the daytime of 08:00-17:00 LT, P_{OH}(HONO) accounted for 78% of P_{OH}(HONO+O_3) in winter-spring and 26% in summer. The seasonal difference in the relative contribution of HONO and O_3 to OH was the combined effect of the seasonal changes in the concentrations of HONO and O_3 and in the photochemistry. Specifically, HONO showed higher concentrations in winter-spring than in summer, whilst O_3 showed much higher levels in summer than in winter-spring, owing to the seasonal variation of sunlight and hence photochemical processes. To sum up,

HONO plays a significant role in OH formation and hence affects the atmospheric oxidation capacity in both seasons.

Figure 6(c) and (d) display the diurnal OH production rates from HONO and O_3 photolysis in the NBB case and BB case, respectively. Compared with the NBB case, P_{OH}(HONO) in the BB case increased greatly, especially in the morning. P_{OH}(HONO) in the BB case was about five times larger than that in the NBB case with a peak of 5.0 ppbv·h^{-1} in the late morning, and P_{OH}(O_3) in the BB case reached the peak of 3.7 ppbv·h^{-1} around noon with the average value of over two times higher than that in the NBB case. The differences of P_{OH}(HONO) and P_{OH}(O_3) are consistent with the concentration differences of HONO and O_3 between the two cases. In terms of relative contribution, while P_{OH}(HONO) was larger than P_{OH}(O_3) only before 08:00 in the NBB case, P_{OH}(HONO) in the BB case was larger than P_{OH}(O_3) before 10:00 and was over three times higher than P_{OH}(O_3) during 06:00-10:00. These results indicate the significant impacts of BB on HONO and atmospheric oxidation capacity, and BB should be taken into consideration in atmospheric modelling study and pollution control policy-making.

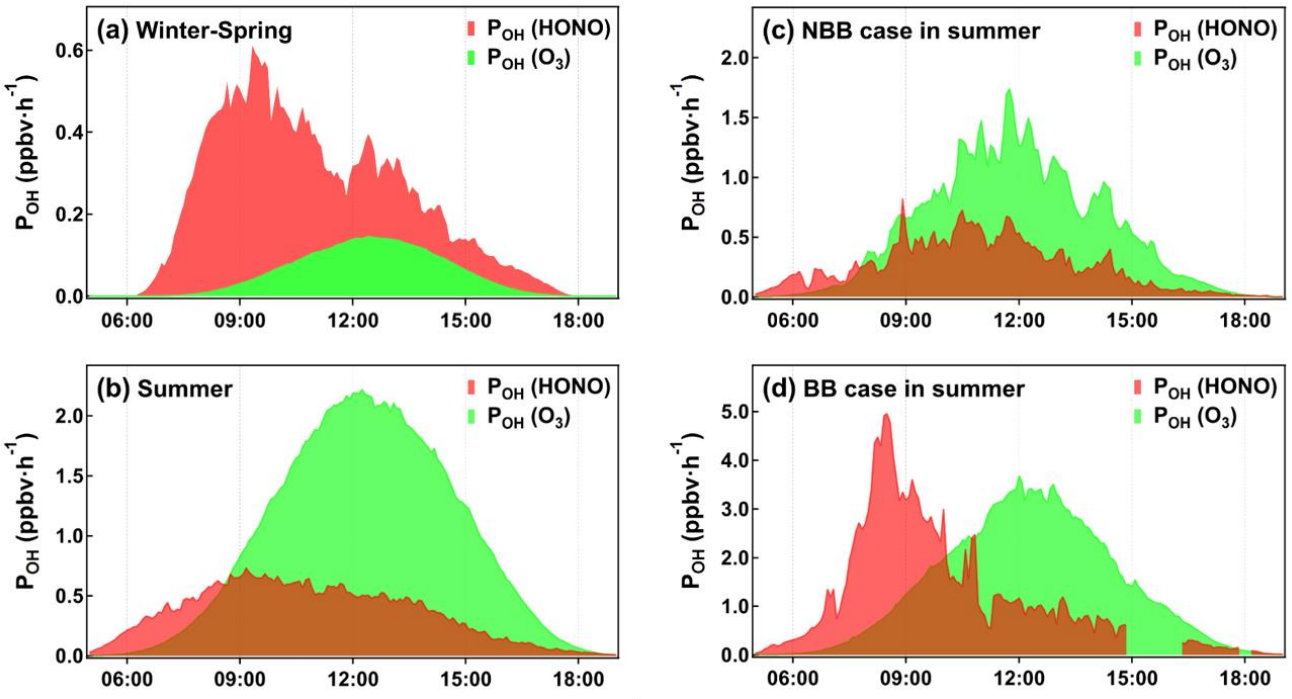

Figure 6. Production rates of OH from the photolysis of HONO and O_3 in (a) winter-spring, (b) summer, (c) the non-biomass burning (NBB) case in summer, and (d) the biomass burning (BB) case in summer.

4. Summary and Conclusions

The paper presents the HONO measured during the winter-spring and summer in 2017 at a rural coastal site in North China and demonstrates the significant seasonal variations in HONO pollution and chemistry, including the pollution characteristics, nocturnal C_{HONO}, daytime budgets, and the impacts on atmospheric oxidation capacity. More severe air pollution was observed in winter-spring than in summer, with the mean HONO mixing ratio of 0.26±0.28 ppbv in winter-spring and 0.17±0.19 ppbv in summer. The HONO/NO_x ratio in summer was about twice of that in winter-spring, and it reached a peak at noon in summer, which indicated the photo-enhanced heterogeneous formation of HONO. The mean nocturnal C_{HONO} in summer was over twice of that in winter-spring. Budget analysis indicated a much stronger daytime P_{other} in summer (0.14-0.56 ppbv·h^{-1}) than in winter-spring (0.02-0.23 ppbv·h^{-1}), and the enhanced photo-induced HONO formation mechanisms were suggested through correlation analysis. Photolysis of nitrate and nitric acid may be the most significant HONO sources, followed by the comparable photo-enhanced heterogeneous conversion of NO_2. HONO photolysis was the major contributor to OH in winter-spring and also a significant OH source in summer. Biomass burning was found to make a significant contribution to HONO through direct HONO emission and aerosol release, which provided HONO precursors and heterogeneous reaction surface. Biomass burning affected HONO chemistry by enhancing the effects of aerosol and weakening the role of photolysis on HONO formation. Besides, HONO photolysis could be enhanced to be the major OH contributor in the morning in the BB case. Therefore, biomass burning should be taken into consideration in HONO study and in making regional pollution control policy, especially during the harvest seasons.

Acknowledgements. The authors are grateful to the Yellow River Delta Ecology Research Station of Coastal Wetland of Chinese Academy of Science and its all staff for offering convenience on our field observation and accommodation, and to the NASA for offering the fire map information.

Funding. This work was supported by the National Natural Science Foundation of China (41675118, 91544213, and 41505111), the Hong Kong Research Grants Council (T24-504/17-N), the Shandong Provincial Natural Science Foundation for Distinguished Young Scholars (ZR2019JQ09), the Qilu Youth Talent Program of Shandong University, and the Jiangsu Collaborative Innovation Center for Climate Change.

References

Acker, K., Febo, A., Trick, S., Perrino, C., Bruno, P., Wiesen, P., Möller, D., Wieprecht, W., Auel, R., Giusto, M., Geyer, A., Platt, U., Allegrini, I., 2006a. Nitrous acid in the urban area of Rome. Atmospheric Environment, 40, 3123-3133. https://doi.org/10.1016/j.atmosenv.2006.01.028

Acker, K., Möller, D., Wieprecht, W., Meixner, F.X., Bohn, B., Gilge, S., Plass-Dülmer, C., Berresheim, H., 2006b. Strong daytime production of OH from HNO_2 at a rural mountain site. Geophysical Research Letters, 33, L02809. https://doi.org/10.1029/2005GL024643

Alicke, B., Platt, U., Stutz, J., 2002. Impact of nitrous acid photolysis on the total hydroxyl radical budget during the Limitation of Oxidant Production/Pianura Padana Produzione di Ozono study in Milan. Journal of Geophysical Research, 107, 8196. https://doi.org/10.1029/2000JD000075

Atkinson, R., Baulch, D.L., Cox, R.A., Crowley, J.N., Hampson, R.F., Hynes, R.G., Jenkin, M.E., Rossi, M.J., Troe, J., 2004. Evaluated kinetic and photochemical data for atmospheric chemistry: Volume I – gas phase reactions of Ox, HOx, NOx and SOx species. Atmospheric Chemistry and Physics, 4, 1461-1738. https://doi.org/10.5194/acp-4-1461-2004

Bejan, I., Abd El Aal, Y., Barnes, I., Benter, T., Bohn, B., Wiesen, P., Kleffmann, J., 2006. The photolysis of ortho-nitrophenols: a new gas phase source of HONO. Physical Chemistry Chemical Physics, 8, 2028-2035. https://doi.org/10.1039/B516590C

Burling, I.R., Yokelson, R.J., Griffith, D.W.T., Johnson, T.J., Veres, P., Roberts, J.M., Warneke, C., Urbanski, S.P., Reardon, J., Weise, D.R., Hao, W.M., de Gouw, J., 2010. Laboratory measurements of trace gas emissions from biomass burning of fuel types from the southeastern and southwestern United States. Atmospheric Chemistry and Physics, 10, 11115-11130. http://doi.org/10.5194/acp-10-11115-2010

Carr, S., Heard, D.E., Blitz, M.A., 2009. Comment on "Atmospheric hydroxyl radical production from electronically excited NO2 and H2O". Science, 324, 336b. https://doi.org/10.1126/science.1166669

Finlayson-Pitts, B.J., Pitts, J.N., 2000. Chemistry of the Upper and Lower Atmosphere, Academic Press, San Diego. http://www.sciencedirect.com/science/article/pii/B9780122570605500009

Finlayson-Pitts, B.J., Wingen, L.M., Sumner, A.L., Syomin, D., Ramazan, K.A., 2003. The heterogeneous hydrolysis of NO2 in laboratory systems and in outdoor and indoor atmospheres: An integrated mechanism. Physical Chemistry Chemical Physics, 5, 223-242. https://doi.org/10.1039/B208564J

Fu, X., Wang, T., Zhang, L., Li, Q., Wang, Z., Xia, M., Yun, H., Wang, W., Yu, C., Yue, D., Zhou, Y., Zheng, J., Han, R., 2019. The significant contribution of HONO to secondary pollutants during a severe winter pollution event in southern China. Atmospheric Chemistry and Physics, 19, 1-14. https://doi.org/10.5194/acp-19-1-2019

Gen, M., Zhang, R., Huang, D., Li, Y. Chan, C., 2019. Heterogeneous Oxidation of SO_2 in Sulfate Production during Nitrate Photolysis at 300 nm: Effect of pH, Relative Humidity, Irradiation Intensity,

and the Presence of Organic Compounds, Environmental Science & Technology 2019 53 (15), 8757-8766. DOI: 10.1021/acs.est.9b01623

Han, C., Yang, W., Yang, H., Xue, X., 2017. Enhanced photochemical conversion of NO_2 to HONO on humic acids in the presence of benzophenone. Environ Pollut, 231, 979-986. https://doi.org/10.1016/j.envpol.2017.08.107

Harrison, R.M., Peak, J.D., Collins, G.M., 1996. Tropospheric cycle of nitrous acid. Journal of Geophysical Research: Atmospheres, 101, 14429-14439. https://doi.org/10.1029/96JD00341

Heland, J., Kleffmann, J., Kurtenbach, R., Wiesen, P., 2001. A new instrument to measure gaseous nitrous acid (HONO) in the atmosphere. Environmental Science and Technology, 35, 3207-3212. https://doi.org/10.1021/es000303t

Kleffmann, J., Benter, T., Wiesen, P., 2004. Heterogeneous reaction of nitric acid with nitric oxide on glass surfaces under simulated atmospheric conditions. The Journal of Physical Chemistry A, 108, 5793-5799. https://doi.org/10.1021/jp040184u

Lammel, G., Cape, J.N., 1996. Nitrous acid and nitrite in the atmosphere. Chemical Society Reviews, 25, 361-369. https://doi.org/10.1039/CS9962500361

Li, D., Xue, L., Wen, L., Wang, X., Chen, T., Mellouki, A., Chen, J., Wang, W., 2018. Characteristics and sources of nitrous acid in an urban atmosphere of northern China: Results from 1-yr continuous observations. Atmospheric Environment, 182, 296-306. https://doi.org/10.1016/j.atmosenv.2018.03.033

Li, S., Matthews, J., Sinha, A., 2008. Atmospheric hydroxyl radical production from electronically excited NO2 and H2O. Science, 319, 1657-1660. https://doi.org/10.1126/science.1151443

Li, X., Brauers, T., Häseler, R., Bohn, B., Fuchs, H., Hofzumahaus, A., Holland, F., Lou, S., Lu, K.D., Rohrer, F., Hu, M., Zeng, L.M., Zhang, Y.H., Garland, R.M., Su, H., Nowak, A., Wiedensohler, A., Takegawa, N., Shao, M., Wahner, A., 2012. Exploring the atmospheric chemistry of nitrous acid (HONO) at a rural site in Southern China. Atmospheric Chemistry and Physics, 12, 1497-1513. http://doi.org/10.5194/acp-12-1497-2012

Liang, Y., Zha, Q., Wang, W., Cui, L., Lui, K.H., Ho, K.F., Wang, Z., Lee, S.-C., Wang, T., 2017. Revisiting nitrous acid (HONO) emission from on-road vehicles: A tunnel study with a mixed fleet. J Air Waste Manag Assoc, 67, 797-805. https://doi.org/10.1080/10962247.2017.1293573

Liu, Y., Lu, K., Ma, Y., Yang, X., Zhang, W., Wu, Y., Peng, J., Shuai, S., Hu, M., Zhang, Y., 2017. Direct emission of nitrous acid (HONO) from gasoline cars in China determined by vehicle chassis dynamometer experiments. Atmospheric Environment, 169, 89-96. https://doi.org/10.1016/j.atmosenv.2017.07.019

Liu, Y., Nie, W., Xu, Z., Wang, T., Wang, R., Li, Y., Wang, L., Chi, X., Ding, A., 2019. Contributions of different sources to nitrous acid (HONO) at the SORPES station in eastern China: results from one-year continuous observation. Atmospheric Chemistry and Physics Discussions, 1-47. https://doi.org/10.5194/acp-2019-219

Meusel, H., Kuhn, U., Reiffs, A., Mallik, C., Harder, H., Martinez, M., Schuladen, J., Bohn, B., Parchatka, U., Crowley, J.N., Fischer, H., Tomsche, L., Novelli, A., Hoffmann, T., Janssen, R.H.H., Hartogensis, O., Pikridas, M., Vrekoussis, M., Bourtsoukidis, E., Weber, B., Lelieveld, J., Williams, J., Pöschl, U., Cheng, Y., Su, H., 2016. Daytime formation of nitrous acid at a coastal remote site in Cyprus indicating a common ground source of atmospheric HONO and NO. Atmospheric Chemistry and Physics, 16, 14475-14493. https://doi.org/10.5194/acp-16-14475-2016

Monge, M.E., D'Anna, B., Mazri, L., Giroir-Fendler, A., Ammann, M., Donaldson, D.J., George, C., 2010. Light changes the atmospheric reactivity of soot. Proceedings of the National Academy of Sciences, 107, 6605-6609. http://doi.org/10.1073/pnas.0908341107

Nie, W., Ding, A.J., Xie, Y.N., Xu, Z., Mao, H., Kerminen, V.M., Zheng, L.F., Qi, X.M., Huang, X., Yang, X.Q., Sun, J.N., Herrmann, E., Petäjä, T., Kulmala, M., Fu, C.B., 2015. Influence of biomass burning plumes on HONO chemistry in eastern China. Atmospheric Chemistry and Physics, 15, 1147-1159. https://doi.org/10.5194/acp-15-1147-2015

Oswald, R., Behrendt, T., Ermel, M., Wu, D., Su, H., Cheng, Y., Breuninger, C., Moravek, A., Mougin, E., Delon, C., Loubet, B., Pommerening-Röser, A., Sörgel, M., Pöschl, U., Hoffmann, T., Andreae, M.O., Meixner, F.X., Trebs, I., 2013. HONO emissions from soil bacteria as a major source of atmospheric reactive nitrogen. Science, 341, 1233-1235. http://doi.org/10.1126/science.1242266

Ren, X., Harder, H., Martinez, M., Lesher, R.L., Oliger, A., Simpas, J.B., Brune, W.H., Schwab, J.J., Demerjian, K.L., He, Y., Zhou, X., Gao, H., 2003. OH and HO_2 chemistry in the urban atmosphere of New York City. Atmospheric Environment, 37, 3639-3651. https://doi.org/10.1016/S1352-2310(03)00459-X

Rohrer, F., Berresheim, H., 2006. Strong correlation between levels of tropospheric hydroxyl radicals and solar ultraviolet radiation. Nature, 442, 184-187. https://doi.org/10.1038/nature04924

Sörgel, M., Regelin, E., Bozem, H., Diesch, J.M., Drewnick, F., Fischer, H., Harder, H., Held, A., Hosaynali-Beygi, Z., Martinez, M., Zetzsch, C., 2011. Quantification of the unknown HONO daytime source and its relation to NO_2. Atmospheric Chemistry and Physics, 11, 10433-10447. http://doi.org/10.5194/acp-11-10433-2011

Sakamaki, F., Hatakeyama, S., Akimoto, H., 1983. Formation of nitrous acid and nitric oxide in the heterogeneous dark reaction of nitrogen dioxide and water vapor in a smog chamber. International Journal of Chemical Kinetics, 15, 1013-1029. https://doi.org/10.1002/kin.550151006

Saliba, N.A., Yang, H., Finlayson-Pitts, B.J., 2001. Reaction of gaseous nitric oxide with nitric acid on silica surfaces in the presence of water at room temperature. The Journal of Physical Chemistry A, 105, 10339-10346. https://doi.org/10.1021/jp012330r

Stemmler, K., Ammann, M., Donders, C., Kleffmann, J., George, C., 2006. Photosensitized reduction of nitrogen dioxide on humic acid as a source of nitrous acid. Nature, 440, 195-198. https://doi.org/10.1038/nature04603

Su, H., Cheng, Y.F., Cheng, P., Zhang, Y.H., Dong, S.F., Zeng, L.M., Wang, X.S., Slanina, J., Shao, M., Wiedensohler, A., 2008a. Observation of nighttime nitrous acid (HONO) formation at a non-urban site during PRIDE-PRD2004 in China. Atmospheric Environment, 42, 6219-6232. https://doi.org/10.1016/j.atmosenv.2008.04.006

Su, H., Cheng, Y.F., Shao, M., Gao, D.F., Yu, Z.Y., Zeng, L.M., Slanina, J., Zhang, Y.H., Wiedensohler, A., 2008b. Nitrous acid (HONO) and its daytime sources at a rural site during the 2004 PRIDE-PRD experiment in China. Journal of Geophysical Research: Atmospheres, 113, D14312. https://doi.org/10.1029/2007JD009060

Wang, J., Zhang, X., Guo, J., Wang, Z., Zhang, M., 2017. Observation of nitrous acid (HONO) in Beijing, China: Seasonal variation, nocturnal formation and daytime budget. Science of the Total Environment, 587-588, 350-359. https://doi.org/10.1016/j.scitotenv.2017.02.159

Wang, S., Zhou, R., Zhao, H., Wang, Z., Chen, L., Zhou, B., 2013. Long-term observation of atmospheric nitrous acid (HONO) and its implication to local NO2 levels in Shanghai, China. Atmospheric Environment, 77, 718-724. https://doi.org/10.1016/j.atmosenv.2013.05.071

Xu, Z., Wang, T., Wu, J., Xue, L., Chan, J., Zha, Q., Zhou, S., Louie, P.K.K., Luk, C.W.Y., 2015. Nitrous acid (HONO) in a polluted subtropical atmosphere: Seasonal variability, direct vehicle emissions and heterogeneous production at ground surface. Atmospheric Environment, 106, 100-109. https://doi.org/10.1016/j.atmosenv.2015.01.061

Xue, L., Gu, R., Wang, T., Wang, X., Saunders, S., Blake, D., Louie, P.K.K., Luk, C.W.Y., Simpson, I., Xu, Z., Wang, Z., Gao, Y., Lee, S., Mellouki, A., Wang, W., 2016. Oxidative capacity and radical chemistry in the polluted atmosphere of Hong Kong and Pearl River Delta region: analysis of a severe photochemical smog episode. Atmospheric Chemistry and Physics, 16, 9891-9903. https://doi.org/10.5194/acp-16-9891-2016

Yang, Q., Su, H., Li, X., Cheng, Y., Lu, K., Cheng, P., Gu, J., Guo, S., Hu, M., Zeng, L., Zhu, T., Zhang, Y., 2014. Daytime HONO formation in the suburban area of the megacity Beijing, China. Science China Chemistry, 57, 1032-1042. https://doi.org/10.1007/s11426-013-5044-0

Yang, W., Han, C., Yang, H., Xue, X., 2018. Significant HONO formation by the photolysis of nitrates in the presence of humic acids. Environ Pollut, 243, 679-686. https://doi.org/10.1016/j.envpol.2018.09.039

Ye, C., Gao, H., Zhang, N., Zhou, X., 2016a. Photolysis of nitric acid and nitrate on natural and artificial surfaces. Environmental Science and Technology, 50, 3530-3536. https://doi.org/10.1021/acs.est.5b05032

Ye, C., Zhang, N., Gao, H., Zhou, X., 2017. Photolysis of particulate nitrate as a source of HONO and NOx. Environmental Science and Technology, 51, 6849-6856. https://doi.org/10.1021/acs.est.7b00387

Ye, C., Zhou, X., Pu, D., Stutz, J., Festa, J., Spolaor, M., Cantrell, C., Mauldin, R.L., Weinheimer, A., Haggerty, J., 2015. Comment on "Missing gas-phase source of HONO inferred from Zeppelin measurements in the troposphere". Science, 348, 1326-1326. http://doi.org/10.1126/science.aaa1992

Ye, C., Zhou, X., Pu, D., Stutz, J., Festa, J., Spolaor, M., Tsai, C., Cantrell, C., Mauldin III, R.L., Campos, T., Weinheimer, A., Hornbrook, R.S., Apel, E.C., Guenther, A., Kaser, L., Yuan, B., Karl, T., Haggerty, J., Hall, S., Ullmann, K., Smith, J.N., Ortega, J., Knote, C., 2016b. Rapid cycling of reactive nitrogen in the marine boundary layer. Nature, 532, 489-491. https://doi.org/10.1038/nature17195

Yin, L., Du, P., Zhang, M., Liu, M., Xu, T., Song, Y., 2019. Estimation of emissions from biomass burning in China (2003–2017) based on MODIS fire radiative energy data. Biogeosciences, 16, 1629-1640. https://doi.org/10.5194/bg-16-1629-2019

Yokelson, R.J., Crounse, J.D., DeCarlo, P.F., Karl, T., Urbanski, S., Atlas, E., Campos, T., Shinozuka, Y., Kapustin, V., Clarke, A.D., Weinheimer, A., Knapp, D.J., Montzka, D.D., Holloway, J., Weibring, P., Flocke, F., Zheng, W., Toohey, D., Wennberg, P.O., Wiedinmyer, C., Mauldin, L., Fried, A., Richter, D., Walega, J., Jimenez, J.L., Adachi, K., Buseck, P.R., Hall, S.R., Shetter, R., 2009. Emissions from biomass burning in the Yucatan. Atmospheric Chemistry and Physics, 9, 5785-5812. https://doi.org/10.5194/acp-9-5785-2009

Yu, Y., Galle, B., Panday, A., Hodson, E., Prinn, R., Wang, S., 2009. Observations of high rates of NO_2-HONO conversion in the nocturnal atmospheric boundary layer in Kathmandu, Nepal. Atmospheric Chemistry and Physics, 9, 541-546. https://doi.org/10.5194/acp-9-6401-2009

Yun, H., Wang, Z., Zha, Q., Wang, W., Xue, L., Zhang, L., Li, Q., Cui, L., Lee, S., Poon, S.C.N., Wang, T., 2017. Nitrous acid in a street canyon environment: Sources and contributions to local oxidation capacity. Atmospheric Environment, 167, 223-234. https://doi.org/10.1016/j.atmosenv.2017.08.018

Zhang, B., Tao, F.-M., 2010. Direct homogeneous nucleation of NO_2, H_2O, and NH_3 for the production of ammonium nitrate particles and HONO gas. Chemical Physics Letters, 489, 143-147. http://doi.org/10.1016/j.cplett.2010.02.059

Zhang, L., Wang, T., Zhang, Q., Zheng, J., Xu, Z., Lv, M., 2016. Potential sources of nitrous acid (HONO) and their impacts on ozone: A WRF-Chem study in a polluted subtropical region. Journal of Geophysical Research: Atmospheres, 121, 3645-3662. https://doi.org/10.1002/2015JD024468

Zhang, Y., Sun, J., Zheng, P., Chen, T., Liu, Y., Han, G., Simpson, I.J., Wang, X., Blake, D.R., Li, Z., Yang, X., Qi, Y., Wang, Q., Wang, W., Xue, L., 2019. Observations of C_1-C_5 alkyl nitrates in the Yellow River Delta, northern China: Effects of biomass burning and oil field emissions. Science of the Total Environment, 656, 129-139. https://doi.org/10.1016/j.scitotenv.2018.11.208

Zheng, P., Chen, T., Dong, C., Liu, Y., Li, H., Han, G., Sun, J., Wu, L., Gao, X., Wang, X., Qi, Y., Zhang, Q., Wang, W., Xue, L., 2019. Characteristics and sources of halogenated hydrocarbons in the Yellow River Delta region, northern China. Atmospheric Research, 225, 70-80. https://doi.org/10.1016/j.atmosres.2019.03.039

Zhou, X., Gao, H., He, Y., Huang, G., Bertman, S.B., Civerolo, K., Schwab, J., 2003. Nitric acid photolysis on surfaces in low-NOx environments: Significant atmospheric implications. Geophysical Research Letters, 30, 2217. https://doi.org/10.1029/2003GL018620